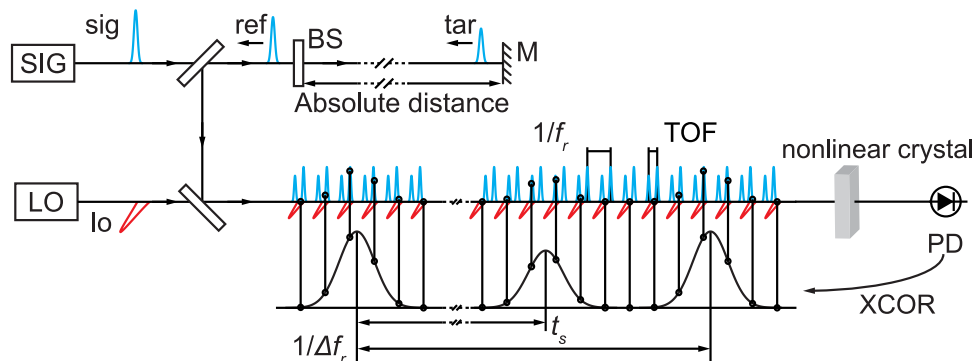


Singular Spectrum Analysis for Extracting Low Amplitude Vibrations in Femtosecond Laser Time-of-Flight Distance Measurements

Volume 13, Number 2, April 2021

Hui Cao
Youjian Song
Minglie Hu
Chingyue Wang



DOI: 10.1109/JPHOT.2021.3057894

Singular Spectrum Analysis for Extracting Low Amplitude Vibrations in Femtosecond Laser Time-of-Flight Distance Measurements

Hui Cao , Youjian Song , Minglie Hu , and Chingyue Wang

Ultrafast Laser Laboratory, Key Laboratory of Opto-electronic Information Technology, Ministry of Education, School of Precision Instruments and Opto-electronics Engineering, Tianjin University, Tianjin 300072, China

DOI:10.1109/JPHOT.2021.3057894

This work is licensed under a Creative Commons Attribution 4.0 License. For more information, see <https://creativecommons.org/licenses/by/4.0/>

Manuscript received December 5, 2020; revised January 11, 2021; accepted February 3, 2021. Date of publication February 9, 2021; date of current version February 26, 2021. This work was sponsored in part by Tianjin Natural Science Foundation under Grant 18JCYBJC16900, in part by the Science and Technology Planning Project of Guangdong Province under Grant 2018B090944001, and in part by the National Natural Science Foundation of China under Grants 61675150, 61827821, 11527808. Corresponding author: Youjian Song (e-mail: yjsong@tju.edu.cn).

Abstract: We utilize singular spectrum analysis (SSA) for post-processing distance measurement data obtained by a dual-comb femtosecond laser rangefinder. Signal denoising technique based on SSA allows detection of low amplitude vibrations from time series of distance data with limited signal-to-noise ratio (SNR). Various one-dimensional vibrations, including harmonic, amplitude modulated harmonic, and sinc-function vibrations, with micrometer amplitude comparable with measurement uncertainty of laser rangefinder, have been imposed on the target mirror by a piezo positioner. These vibrations have been extracted by SSA and the obtained vibration amplitudes agree with that imposed on the target very well. A commercial interferometer is used to evaluate the accuracy of SSA. Standard deviations of residuals between the SSA extractions and interferometer measurements are smaller than $0.6 \mu\text{m}$. This technique is promising for complex moving pattern detection in object tracking and remote sensing.

Index Terms: Absolute distance measurement, femtosecond laser, singular spectrum analysis.

1. Introduction

Non-contact vibration measurement is crucial for a number of industrial applications, such as mechanical damage detection [1], [2], microsystem diagnosis [3] and biomedical imaging [4]. Laser-based distance measurement provides a simple and direct approach to high precision vibration detection [5], [6]. Recently, distance measurement based on femtosecond lasers and optical frequency combs have drawn great attention [7]–[13]. In particular, a dual-comb configuration [14]–[16] allows direct time-of-flight (TOF) absolute distance measurements with large unambiguous range, sub-micrometer precision, high update rate, negligible dead-zone and traceability time-frequency standard [17]–[20]. Several research groups have demonstrated low amplitude vibrational target detections based on a dual-comb laser by exploiting the above advantages [19]–[22].

The high measurement precision allows dual-comb rangefinder to resolve small amplitude vibrations, and the upper limit for the detectable vibration frequency is determined by half of update rate. The moving information will be submerged in noise and cannot be distinguished directly when motion amplitude is comparable with measurement noise. For stationary and uniformly moving targets, multiple averaging can be applied to significantly reduce measurement noise at the expense of update rate, while this method fails for complex vibrations.

Kalman filtering (KF) is appropriate to solve this problem [23], [24]. Target motions can be extracted from measurement noise without loss of update rate, even for irregularly moving and vibrating targets. However, this method is only effective in the presence of Gaussian measurement noise with known intensity. The prior knowledge of predicted motion model is also essential. KF's estimation of the state is determined by previous state and innovation [25]. When applied in ranging, the innovation only has distance, and does not include velocity and acceleration. The estimation of distance should be determined by distance, velocity and acceleration, which means that there will be inevitable delay in state estimation. However, the delay can be reduced rather than eliminated only when the velocity and acceleration of the target change slowly enough. Moreover, even if the target moving slowly enough, the parameters of the predicted motion model must be identified accurately. Meanwhile, the change of motion mode will make KF invalid.

In the case without motion model and measurement noise information, singular spectrum analysis (SSA) [26]–[30], is capable to separate motion from noise. SSA is a data-driven method for decomposing nonlinear time series into components with certain interpretations such as trend, oscillation or noise. SSA method has been utilized in fields of GPS data processing [27], hyperspectral imaging [31] and economics [32]. Recently, we also apply this method to improve absolute ranging precision of objects with uniform motion [33].

In this work, we utilize a free running dual-comb laser rangefinder to measure a vibrational target. The noisy absolute distance measurements have been processed by SSA, and decomposed into components classified as oscillation and noise, allowing the extraction of target motion from measurement noise. Firstly, we use a commercial interferometer to calibrate the rangefinder. Then several motion modes are imposed on a target mirror by a piezo positioner and measured by the dual-comb rangefinder. Subsequently, SSA is used to process the measured distance series. The vibrations can be extracted out of the measurement noise even when the target motion amplitude is comparable with measurement noise. The retrieved vibrations are compared with the results of the commercial interferometer and agree with the vibrations imposed on the target very well.

2. Absolute Distance Measurement

Absolute distance is measured by a free running dual-comb laser rangefinder based on asynchronous optical sampling (ASOPS) [34]. The principle is shown in Fig. 1, the signal laser (SIG) and the local oscillator (LO) have similar repetition frequencies, f_r and $f_r - \Delta f_r$ respectively. The signal pulse train is split into reference and target by a beam splitter. The time interval between a reference pulse and its adjacent target pulse corresponds to the target time-of-flight. The LO with orthogonal polarization is used to sample envelopes of the reference and the target pulse trains in the nonlinear crystal. The LO pulses walk through the reference and the target pulse due to the slightly different repetition rate Δf_r . The waveforms of the reference and the target pulses are effectively stretched in time domain by $f_r/\Delta f_r$ times through optical intensity cross-correlation (XCOR). The stretched pulses could be detected by standard electronics. The absolute distance measurements are calculated through the stretched envelopes, the repetition rate and air group index:

$$d = \frac{c}{2n_g} \frac{\Delta f_r}{f_r} t_s, \quad (1)$$

where n_g represents air group index.

The experiment setup is shown in Fig. 2. The two femtosecond lasers are free running and working at 1550 nm band, serving as signal laser and local oscillator respectively. The repetition

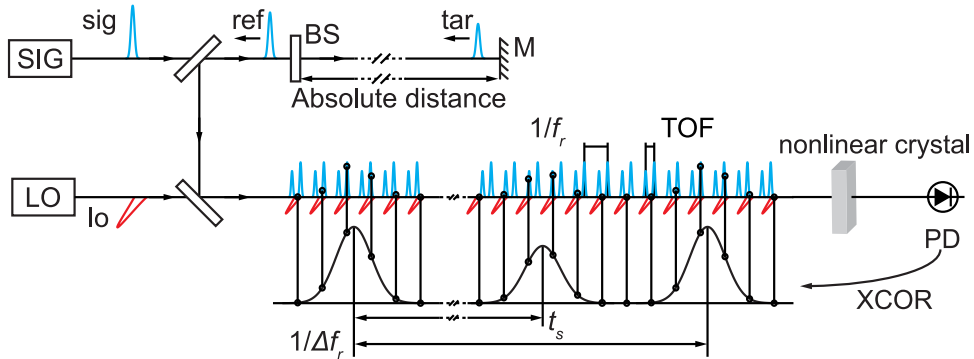


Fig. 1. Schematic diagram of time-of-flight (TOF) absolute distance measurement in a free running dual-comb laser rangefinder. SIG, signal laser; LO, local oscillator; sig, signal pulse; ref, reference pulse; tar, target pulse; BS, beam splitter; M, target mirror; TOF, time-of-flight; XCOR, optical intensity cross-correlation; PD, photodetector.

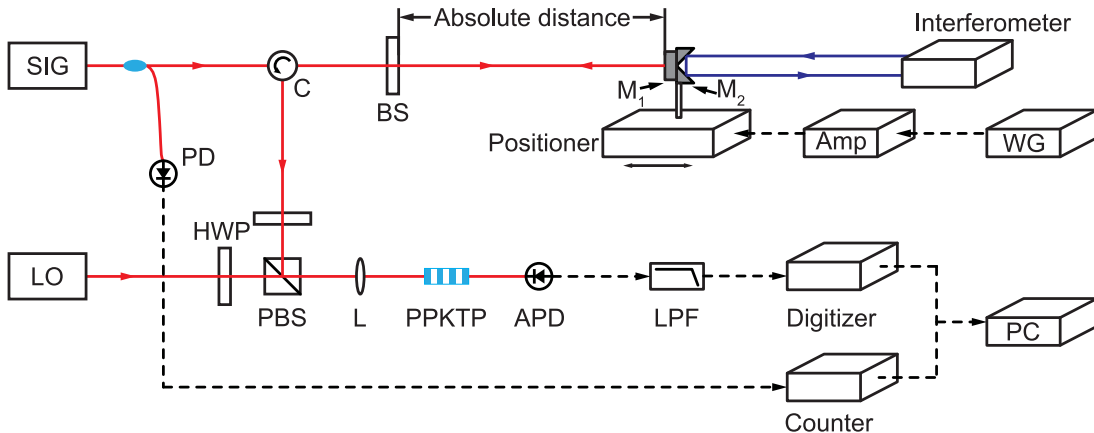


Fig. 2. Femtosecond laser TOF distance measurement setup. Red lines: optical path of free running dual-comb rangefinder; blue lines: optical path of commercial interferometer; dash lines: electrical path. LO, local oscillator; HWP, half wave plate; PBS, polarization beam splitter; L, lens; PPKTP, periodically poled potassium titanyl phosphate; APD, avalanche photodiode; LPF, low pass filter; SIG, signal laser; PD, photodiode; C, circulator; BS, beam splitter; M₁, target mirror of free running dual-comb laser rangefinder; M₂, target mirror of commercial interferometer; Positioner, piezo positioner; Amp, voltage amplifier; WG, arbitrary waveform generator.

rates of lasers are at approximately 73.6 MHz. The repetition rates difference between two lasers is 2 kHz. The signal laser beam is split into two parts by a partial reflector with a transmission of 70%. The reflected beam serves as reference, while the transmitted beam is directed to a target mirror. The distance between the beam splitter and the target mirror is the desired absolute distance. The reflected reference beam and target beam are combined with the local oscillator beam at the polarizing beam splitter (PBS). The combined beam emits to a lens and focused on a periodically poled potassium titanyl phosphate (PPKTP) crystal for asynchronous optical sampling by type-II sum frequency generation (SFG). The intensity cross correlation pulses generated by SFG have durations of nanosecond-level, which can be detected by a photodetector directly. A low pass filter of 32 MHz is used to extract the envelopes of the generated intensity cross correlation pulses by PPKTP. The envelopes are detected by an avalanche photodiode (APD). The analog envelopes are sampled continuously by a data acquisition card (National Instrument, PXIe-5122)

with a resolution of 14-bit and sampling rate of 100 MHz. Since the limitation of the cache in the data acquisition card, the maximum sampling rate of the absolute distance, which is determined by the repetition rates difference Δf_r , cannot be reached. For long time sampling, we sample the digital envelopes at every 5 ms, i.e., the sampling rate of absolute distance is set to 200 Hz. The digital envelopes are immediately used to calculate the pulse peak moment through Gaussian curve fitting, then the absolute distance is obtained according to the Eq. 1. Meanwhile, the repetition rate f_r is measured by a commercial frequency counter (Agilent, 53220 A).

The target mirror is fixed on a piezo positioner (piezosystemjena, PX100) to implement movements. The base line of the rangefinder and the piezo positioner axis of motion are parallel. A waveform generator connects to a voltage amplifier (piezosystemjena, ENV40), which drives the piezo positioner to vibrate along its axis. A commercial laser interferometer (Renishaw, XL-80) is used to comparison. Another retro-reflector and the target mirror of the rangefinder are fixed back together. An arbitrary waveform generator produces vibrations to drive the voltage amplifier. The vibrations are measured by the rangefinder and the interferometer, and the measurements are subsequently processed by SSA.

3. Singular Spectrum Analysis

Data obtained by the rangefinder will be processed by SSA to extract the moving information. The obtained data of absolute distances $\mathbf{d} = [d_0, \dots, d_{N-1}]$ over a certain sampling time serves as the input signal of SSA, where N is the total sample number. The procedure of SSA is divided into two steps: decomposition and reconstruction. In decomposition, the first step is to embed the one-dimensional input signal into an L -dimensional phase space by using lagged vectors. The lagged vectors $\{\mathbf{d}(n) = d_n, \dots, d_{n+L-1} : n = 0, \dots, N-L\}$ are delayed slices of the input signal. The projection, i.e., the trajectory matrix \mathbf{X} , is formed by concatenating the lagged vectors. Thus, the input signal is transformed into the trajectory matrix as follows:

$$\mathbf{X} = \begin{pmatrix} d_0 & \cdots & d_{L-1} \\ \vdots & \ddots & \vdots \\ d_{N-L} & \cdots & d_{N-1} \end{pmatrix}. \quad (2)$$

The second step is to obtain singular value decomposition (SVD) of the trajectory matrix \mathbf{X} :

$$\mathbf{X} = \mathbf{U}\Sigma\mathbf{V}^T, \quad (3)$$

where $(\cdot)^T$ is the transpose operation. The decomposition can be expressed by the sum of components:

$$\mathbf{X} = \sum_{k=1}^L \mathbf{u}_k \sigma_k \mathbf{v}_k^T, \quad (4)$$

where σ_k , \mathbf{u}_k and \mathbf{v}_k are the i -th diagonal element of Σ , column vectors of \mathbf{U} and \mathbf{V} respectively. $\{\mathbf{u}_k, \sigma_k, \mathbf{v}_k\}$ presents k -th eigen pair in the sum. The eigen pairs are sorted by descending order of the singular values σ .

While in reconstruction, the eigen pairs are grouped and used to reconstruct signal. Since each item of the sum in Eq. (4) has a same size with \mathbf{X} , diagonal averaging, the reverse operation of signal embedding, averaging the elements on skew diagonals of matrix, is used to obtain reconstructed components (RCs) of the signal. The k -th RC is obtained by

$$rc_n^{(k)} = \begin{cases} \frac{1}{n+1} \sum_{j=0}^n x_{j,n-j}^{(k)}, & 0 \leq n \leq L-1 \\ \frac{1}{L} \sum_{j=0}^{L-1} x_{j,n-j}^{(k)}, & L-1 < n < N-L \\ \frac{1}{N-n} \sum_{j=n-N+L}^{L-1} x_{j,n-j}^{(k)}, & N-L \leq n \leq N-1 \end{cases} \quad (5)$$

where $x_{m,n}^{(k)}$ represents the m -th row, n -th column element of the matrix $\mathbf{u}_k \sigma_k \mathbf{v}_k^T$.

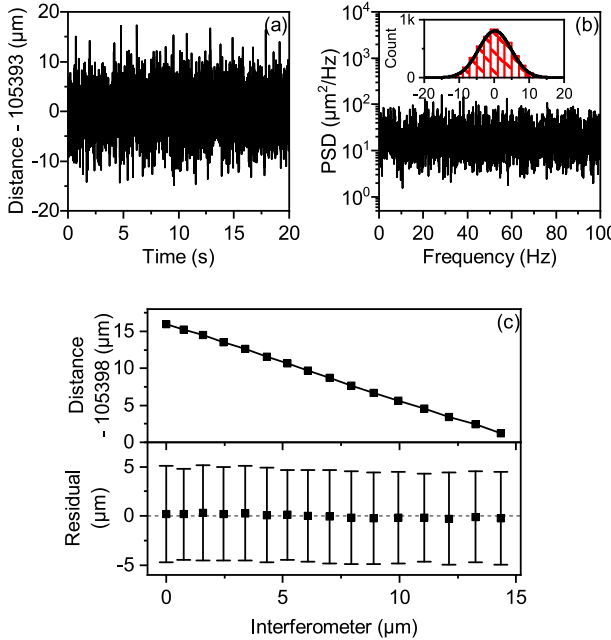


Fig. 3. Stationary measurement. (a) time domain waveform of a 20 s measurement; (b) power spectral density of (a); subfigure of (b) histogram of (a); (c) comparison between the rangefinder and the interferometer.

Finally, the RCs will be grouped into certain subsets. If \mathbf{K} is a subset whose corresponding RCs is grouped as signal, then the reconstructed signal sig is

$$sig = \sum_{k \in \mathbf{K}} RC^{(k)}. \quad (6)$$

Generally, the sum of the leading RCs accounts for the largest contribution of the original signal. A harmonic vibration can be decomposed into two orthogonal RCs, that is, RC1 and RC2. An amplitude-modified (AM) vibration has three frequencies, which are the center frequency and two side frequencies. As a result, the AM vibration can be reconstructed by RC1 to RC6.

4. Experiment Result

The first experiment is to measure the distance when the target is stationary. The target is placed approximately at 0.105 m. Fig. 3(a) shows a 20 s time domain waveform of the rangefinder, which has a mean of 105413.20 μm and an uncertainty of 4.64 μm. Fig. 3(b) and its subfigure are power spectral density (PSD) and histogram of the time domain waveform in Fig. 3(a) respectively, which shows a Gaussian white noise in the rangefinder. Fig. 3(c) shows the comparison between the rangefinder and the interferometer at different positions of the platform. The platform has moved from 0 μm to 15 μm, with a step of 1 μm. As the distance changes, the difference between the two methods remains basically unchanged, the residuals of the rangefinder are less than 0.3 μm and the uncertainties are approximately 4.70 μm.

The performance of SSA is firstly demonstrated by extracting a harmonic vibration. The frequency of the vibration is set to 1 Hz with an peak-to-peak amplitude of 15 μm. The absolute distances of the target mirror with the harmonic vibration are sampled continuously in 10 s. Fig. 4(a) shows that the vibration is submerged in noise and it is hard to distinguish the vibration from noise base in time domain. By using SSA, the vibration is separated from the noisy signal and shown as red curve in the Fig. 4(a). The residual in Fig. 4(a) is the difference between the SSA extraction and

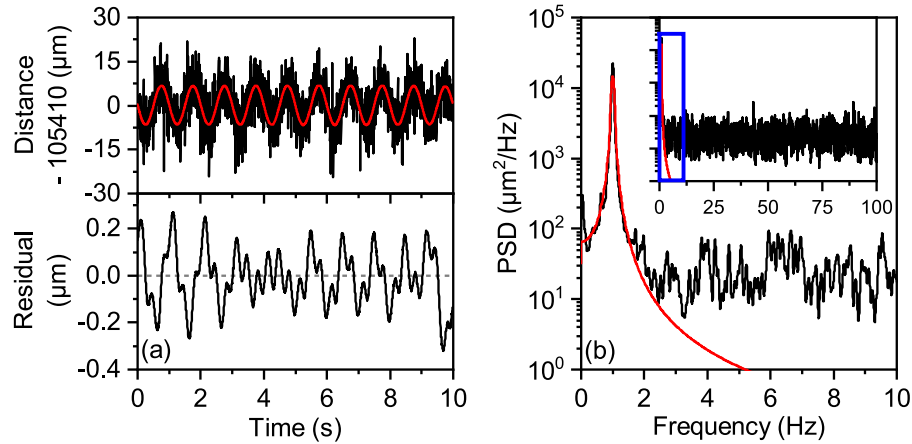


Fig. 4. Harmonic vibration, frequency 1 Hz, peak-to-peak amplitude 15 μm . Black curve: the measurements of the free running dual-comb rangefinder, red curve: SSA extraction of the measurements by the rangefinder. (a) time domain and residual of SSA result against interferometer result; (b) power spectral density.

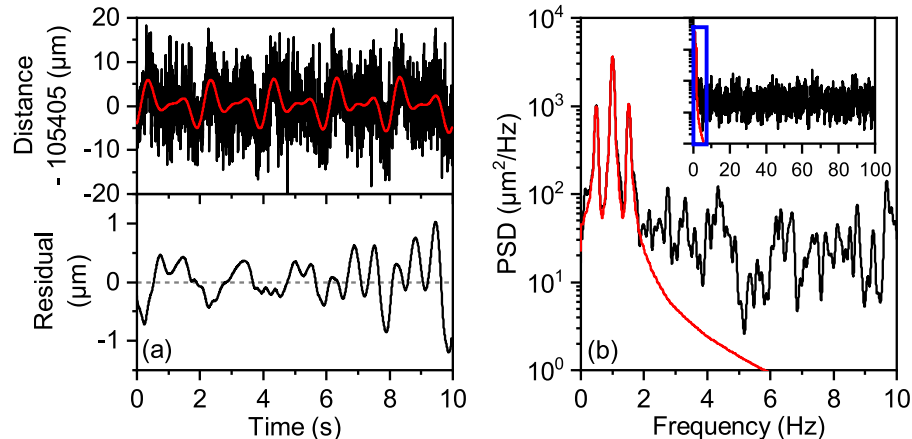


Fig. 5. Amplitude-modified vibration. Center frequency: 1 Hz, modulation frequency: 0.5 Hz, modulation depth 100%, peak-to-peak amplitude 15 μm . Black curve: the measurements of the free running dual-comb rangefinder, red curve: SSA extraction of the measurements by the rangefinder. (a) time domain and residual of SSA result against interferometer result; (b) power spectral density.

the interferometer measurements which has a standard deviation of 0.1180 μm . Fig. 4(b) and its subfigure are the PSD of the original measurements and the SSA extraction. The PSD shows that the vibration is extracted out of the Gaussian white noise in the rangefinder. The extracted vibration has a frequency of 0.9984 Hz.

An AM harmonic vibration is demonstrated to show the capacity of SSA for extracting a modulated harmonic vibration. The carrier harmonic has a frequency of 1 Hz and the modulation frequency is set to 0.5 Hz with a modulation depth of 100%. That is, three frequencies of 0.5, 1, 1.5 Hz are in the vibration. The peak-to-peak amplitude is set to 15 μm . The obtained noisy AM vibration is shown in Fig. 5(a) and the vibration is completely invisible from the time domain waveform. Three frequency components are decomposed by the SSA and their sum is reconstructed as the AM vibration, shown as red curve in Fig. 5(a). The residual of the SSA reconstruction is 0.3781 μm . Fig. 5(b) shows the PSD of the original measurements and the SSA reconstruction. All

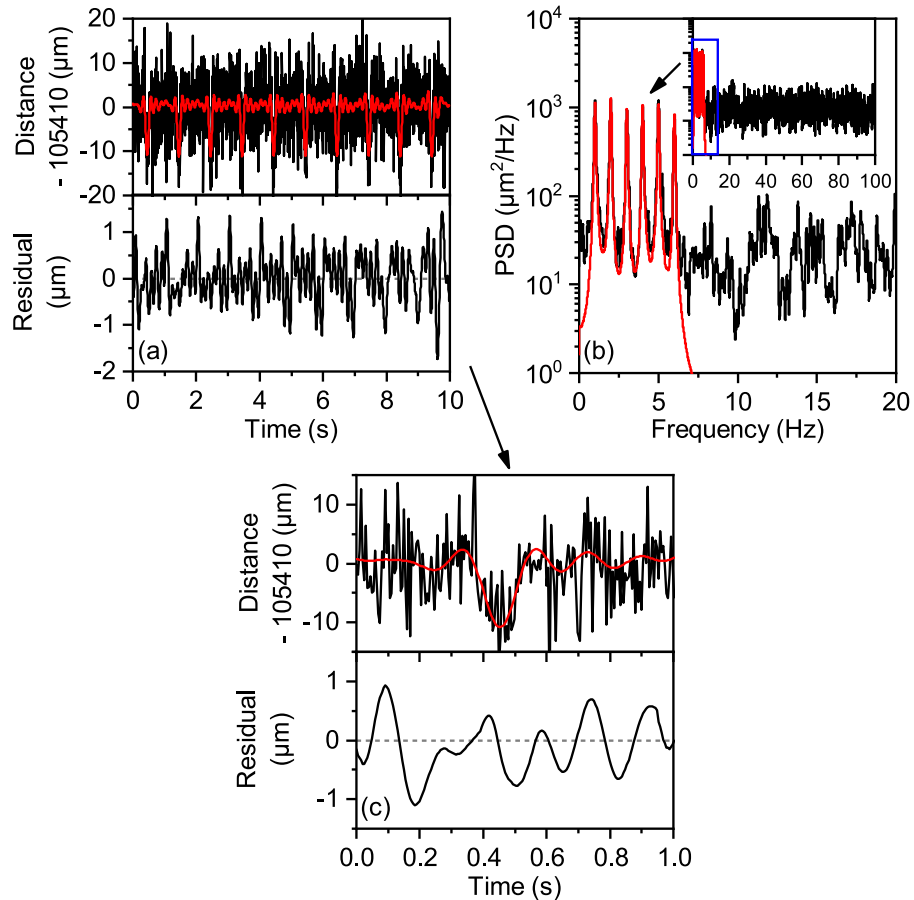


Fig. 6. Sinc-function vibration. Repetition frequency: 10 Hz, peak-to-peak amplitude 15 μm . Black curve: the measurements of the free running dual-comb rangefinder, red curve: SSA extraction of the measurements by the rangefinder. (a) time domain and residual of SSA result against interferometer result; (b) power spectral density; (c) one cycle time domain and residual of SSA result.

three frequencies are reserved and the Gaussian white noise is separated out of the vibration. The three frequencies in the SSA reconstruction are 0.4898, 0.9998, and 1.5120 Hz respectively.

Next, a sinc-function vibration is used to demonstrate the capacity of SSA for processing a more complex vibration. The sinc-function vibration has a peak-to-peak amplitude of 15 μm and a repetition frequency of 10 Hz. As is shown in Fig. 6(a), the side lobes of the sinc-function can be barely recognized. The red curve in Fig. 6(a) shows the SSA reconstruction of the sinc-function vibration. The residual of the result is 0.5337 μm . Fig. 6(b) shows the PSD of the original measurements and the SSA reconstruction. Six frequency peaks are in the PSD and the SSA reconstruction captures all the peaks. The six frequencies in the SSA reconstruction are 1.0001, 1.9953, 3.0043, 4.0017, 5.0010, and 6.0037 Hz respectively. Fig. 7 shows the leading 12 RCs of the sinc-function vibration in Fig. 6, which are used to reconstruct the sinc-function vibration.

Finally, a 100 Hz vibration is introduced to illustrate the applicability of SSA to extract vibrations with different frequencies. Due to the positioner with loaded reflectors cannot vibrate with such a frequency, a piezo actuator (Physik Instrumente, P-840.2) is used to replace the positioner and generate the 100 Hz vibration. The peak-to-peak amplitude of the vibration is set to 12 μm . Meanwhile, the vibration cannot be captured under the sampling rate of the rangefinder in real-time mode. Therefore, to measure the vibration, the maximum sampling rate of the rangefinder is necessary. The envelopes are firstly sampled by the data acquisition card continuously in 1 s,

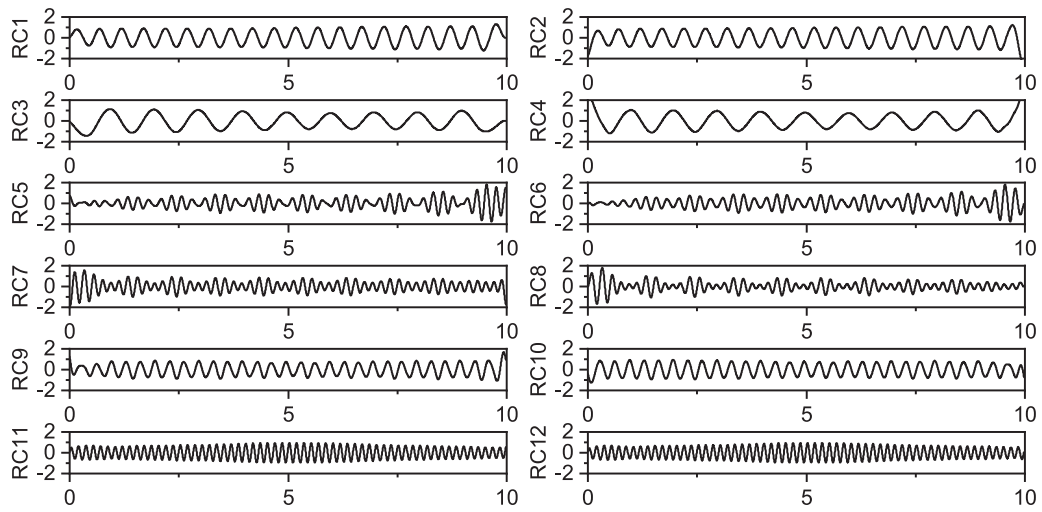


Fig. 7. The leading 12 reconstructed components (RCs) of the sinc-function vibration in Fig. 6. The sum of RC1 to RC12 is the reconstructed vibration.

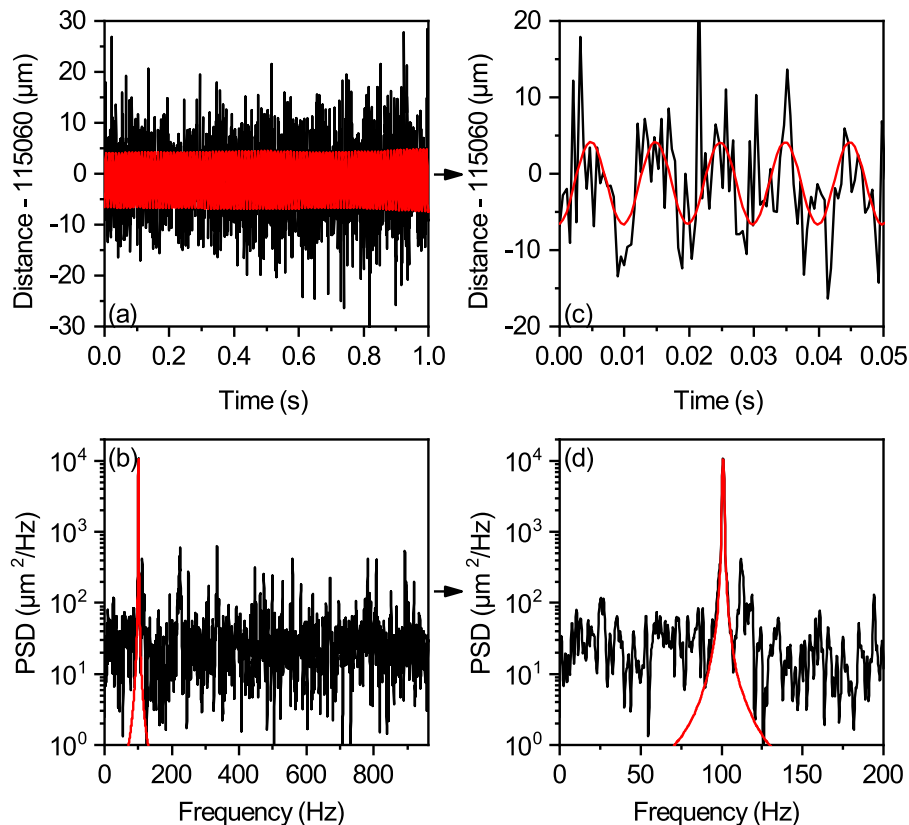


Fig. 8. 100 Hz vibration with peak-to-peak amplitude of $12 \mu\text{m}$. Black curve: the measurements of the free running dual-comb rangefinder; red curve: SSA extraction. (a) time domain, (b) power spectral density; (c) time domain from 0 s to 0.05 s; (d) PSD from 0 Hz to 200 Hz.

and then stored for the following absolute distance calculation, rather than calculating the absolute distance in real-time. Fig. 4(a) shows the measured 100 Hz vibration by the rangefinder and the extraction by SSA in time domain. Fig. 4(b) is PSD of the measurements and the extraction. Fig. 4(c) and (d) are time domain from 0 s to 0.05 s and PSD from 0 Hz to 200 Hz respectively. The extracted vibration has a frequency of 100.46 Hz.

5. Discussion and Conclusion

For same window length and signal length, the errors introduced by each RC are approximately same. If a vibration is reconstructed by a more RCs, the residual will have a larger error. A harmonic vibration will be decomposed into two orthogonal RCs, while an AM-vibration and a sinc-vibration have multiple harmonics, 3 harmonics and 6 harmonics respectively, which means the AM and sinc vibrations are reconstructed by RC1-RC6 and RC1-RC12 respectively. Theoretically, the errors of reconstructed AM and sinc vibrations will be 3 times and 6 times of the error of harmonic vibration. The actual standard deviations of residuals of the AM vibration and the sinc vibration are 3.2 and 4.5 times of the harmonic vibration, respectively. The residual of the sinc-vibration is smaller than the theoretical value, since the errors of RC1-RC12 are partially offset from each other.

In summary, we introduce SSA method to improve the precision for small amplitude vibration measurements based on femtosecond laser absolute ranging. Experiments show that SSA allows accurate extraction of vibration modes with few micrometers amplitude from low SNR distance measurement data without losing details. The residuals of the SSA reconstructions are smaller than $0.6 \mu\text{m}$. This technique can be applied to various laser vibrometric scenarios, where high precision extraction of both the vibration mode and location of the vibrating object is required.

5. Acknowledgment

The authors wish to thank Xu Liang and Prof. Linghui Yang for providing the laser interferometer and valuable technical support.

References

- [1] X. Fang and J. Tang, "Damage detection by statistical analysis of vibration signature," in *Proc. Smart Structures Mater.: Sensors Smart Structures Technol. Civil, Mech. Aerosp. Syst.*, May 2005, pp. 802–810.
- [2] S. Orhan, N. Aktürk, and V. Çelik, "Vibration monitoring for defect diagnosis of rolling element bearings as a predictive maintenance tool: Comprehensive case studies," *Ndt & E Int.*, vol. 39, no. 4, pp. 293–298, Jun. 2006.
- [3] J. Feldman *et al.*, "Vibration-based diagnostics for rotary MEMS," *J. Microelectromech. Syst.*, vol. 24, no. 2, pp. 289–299, Apr. 2015.
- [4] B. F. Kennedy, M. Wojtkowski, M. Szkulmowski, K. M. Kennedy, K. Karnowski, and D. D. Sampson, "Improved measurement of vibration amplitude in dynamic optical coherence elastography," *Biomed. Opt. Exp.*, vol. 3, no. 12, Dec. 2012, Art. no. 3138.
- [5] N. Kuse, A. Ozawa, and Y. Kobayashi, "Static FBG strain sensor with high resolution and large dynamic range by dual-comb spectroscopy," *Opt. Exp.*, vol. 21, no. 9, 2013, Art. no. 11141.
- [6] Y. Na *et al.*, "Ultrafast, sub-nanometre-precision and multifunctional time-of-flight detection," *Nat. Photon.*, vol. 14, no. 6, pp. 355–360, 2020.
- [7] K. Minoshima and H. Matsumoto, "High-accuracy measurement of 240-m distance in an optical tunnel by use of a compact femtosecond laser," *Appl. Opt.*, vol. 39, no. 30, Oct. 2000, Art. no. 5512.
- [8] H. Wu *et al.*, "Absolute distance measurement using frequency comb and a single-frequency laser," *IEEE Photon. Technol. Lett.*, vol. 27, no. 24, pp. 2587–2590, Dec. 2015.
- [9] J. Kim and Y. Song, "Ultralow-noise mode-locked fiber lasers and frequency combs: Principles, status, and applications," *Adv. Opt. Photon.*, vol. 8, no. 3, Sep. 2016, Art. no. 465.
- [10] H. Shi *et al.*, "Review of low timing jitter mode-locked fiber lasers and applications in dual-comb absolute distance measurement," *Nanotechnol. Precis. Eng.*, vol. 1, no. 4, pp. 205–217, Dec. 2018.
- [11] Y. S. Jang and S. W. Kim, "Distance measurements using mode-locked lasers: A review," *Nanomanufacturing Metrol.*, vol. 1, no. 3, pp. 131–147, Sep. 2018.
- [12] B. Lin *et al.*, "Dual-comb absolute distance measurement based on a dual-wavelength passively mode-locked laser," *IEEE Photon. J.*, vol. 9, no. 6, Dec. 2017, Art. no. 7106508.
- [13] H. Yang, C. Zhao, H. Zhang, Z. Zhang, and K. Gui, "A novel hybrid TOF/phase-shift method for absolute distance measurement using a falling-edge RF-modulated pulsed laser," *Opt. Laser Technol.*, vol. 114, pp. 60–65, Jun. 2019.

- [14] M. Cui *et al.*, "High-accuracy long-distance measurements in air with a frequency comb laser," *Opt. Lett.*, vol. 34, no. 13, Jul. 2009, Art. no. 1982.
- [15] T. Liu, N. R. Newbury, and I. Coddington, "Sub-micron absolute distance measurements in sub-millisecond times with dual free-running femtosecond Er fiber-lasers," *Opt. Exp.*, vol. 19, no. 19, Sep. 2011, Art. no. 18501.
- [16] Y. Liang *et al.*, "1550-nm time-of-flight ranging system employing laser with multiple repetition rates for reducing the range ambiguity," *Opt. Exp.*, vol. 22, no. 4, Feb. 2014, Art. no. 4662.
- [17] J. Lee, K. Lee, S. Lee, S.-W. Kim, and Y.-J. Kim, "High precision laser ranging by time-of-flight measurement of femtosecond pulses," *Meas. Sci. Technol.*, vol. 23, no. 6, Jun. 2012, Art. no. 065203.
- [18] H. Zhang, X. Wu, H. Wei, and Y. Li, "Compact dual-comb absolute distance ranging with an electric reference," *IEEE Photon. J.*, vol. 7, no. 3, Jun. 2015, Art. no. 6801508.
- [19] I. Coddington, W. C. Swann, L. Nenadovic, and N. R. Newbury, "Rapid and precise absolute distance measurements at long range," *Nat. Photon.*, vol. 3, no. 6, pp. 351–356, Jun. 2009.
- [20] J. Lee, Y. Kim, K. Lee, S. H. Lee, and S. Kim, "Time-of-flight measurement with femtosecond light pulses," *Nat. Photon.*, vol. 4, no. 10, pp. 716–720, Oct. 2010.
- [21] Y. Bitou, T. R. Schibli, and K. Minoshima, "Accurate wide-range displacement measurement using tunable diode laser and optical frequency comb generator," *Opt. Exp.*, vol. 14, no. 2, 2006, Art. no. 644.
- [22] S. Boudreau and J. Genest, "Range-resolved vibrometry using a frequency comb in the OSCAT configuration," *Opt. Exp.*, vol. 22, no. 7, 2014, Art. no. 8101.
- [23] L. Tao, Z. Liu, W. Zhang, and Y. Zhou, "Frequency-scanning interferometry for dynamic absolute distance measurement using Kalman filter," *Opt. Lett.*, vol. 39, no. 24, Dec. 2014, Art. no. 6997.
- [24] J. Yu, H. Shi, Y. Song, H. Cao, M. Hu, and Q. Wang, "Study on Kalman filtering in high-precision absolute distance measurement based on dual femtosecond lasers," *Chin. J. Lasers*, vol. 44, no. 6, 2017, Art. no. 0 610001.
- [25] T. Kailath, "The divergence and bhattacharyya distance measures in signal selection," *IEEE Trans. Commun.*, vol. COM-15, no. 1, pp. 52–60, Feb. 1967.
- [26] D. Broomhead and G. P. King, "Extracting qualitative dynamics from experimental data," *Physica D: Nonlinear Phenomena*, vol. 20, no. 2/3, pp. 217–236, Jun. 1986.
- [27] Q. Chen, T. van Dam, N. Sneeuw, X. Collilieux, M. Weigelt, and P. Rebischung, "Singular spectrum analysis for modeling seasonal signals from GPS time series," *J. Geodynamics*, vol. 72, pp. 25–35, Dec. 2013.
- [28] B. Yang, C. Yu, and Y. Dong, "Capacitively coupled electrocardiogram measuring system and noise reduction by singular spectrum analysis," *IEEE Sensors J.*, vol. 16, no. 10, pp. 3802–3810, May 2016.
- [29] A. Maddirala and R. A. Shaik, "Removal of EOG artifacts from single channel EEG signals using combined singular spectrum analysis and adaptive noise canceler," *IEEE Sensors J.*, vol. 16, no. 23, pp. 8279–8287, Dec. 2016.
- [30] N. Golyandina, "Particularities and commonalities of singular spectrum analysis as a method of time series analysis and signal processing," *Wiley Interdiscipl. Rev.: Comput. Statist.*, vol. 12, no. 4, pp. 1–39, 2020.
- [31] J. Zabalza, C. Qing, P. Yuen, G. Sun, H. Zhao, and J. Ren, "Fast implementation of two-dimensional singular spectrum analysis for effective data classification in hyperspectral imaging," *J. Franklin Inst.*, vol. 355, no. 4, pp. 1733–1751, Mar. 2018.
- [32] H. Hassani and A. Zhigljavsky, "Singular spectrum analysis: Methodology and application to economics data," *J. Syst. Sci. Complexity*, vol. 22, no. 3, pp. 372–394, Jun. 2009.
- [33] H. Cao *et al.*, "Reduction of moving target time-of-flight measurement uncertainty in femtosecond laser ranging by singular spectrum analysis based filtering," *Appl. Sci.*, vol. 8, no. 9, Sep. 2018, Art. no. 1625.
- [34] H. Shi, Y. Song, F. Liang, L. Xu, M. Hu, and C. Wang, "Effect of timing jitter on time-of-flight distance measurements using dual femtosecond lasers," *Opt. Exp.*, vol. 23, no. 11, Jun. 2015, Art. no. 14057.